Dalton Transactions

ROYAL SOCIETY OF CHEMISTRY

PAPER

View Article Online
View Journal | View Issue

Cite this: *Dalton Trans.*, 2026, **55**, 8611

Mechanistic implications of excited high-spin states, spin–spin coupling, and differential [2Fe–2S]$^{+}$ cluster temperature relaxations in the electron-bifurcating NfnABC from *Thermococcus sibiricus*

Gregory E. Vansuch, *[a] Shuning Wang,[b] Gerrit J. Schut,[b] Michael W. W. Adams[b] and Carolyn E. Lubner *[a]

Electron bifurcation (EB) is a mechanism of biological energy transduction in which multiple oxidation–reduction (redox) reactions are thermodynamically coupled within a single enzyme, enabling the enzyme to harness the excess free energy from an exergonic process to drive an endergonic process. Because of this unprecedented chemistry, there is interest to translate EB principles to artificial and bioengineered systems, but a hurdle is that knowledge pertaining to the fundamental design principles of EB enzymes remains scarce. Here, we investigated the fundamental physical and electronic properties of electron transfer sites in a spectroscopically uncharacterized member of the BfuABC family of EB enzymes, the NADH-dependent reduced-ferredoxin:NADP^{+} oxidoreductase from *Thermococcus sibiricus* (*Tsi* NfnABC). Cryo-EM structures of *Tsi* NfnABC previously demonstrated that it contains twelve redox cofactors: two flavins (one FAD and one FMN), eight [4Fe–4S] clusters, and two [2Fe–2S] clusters. The FMN, one [4Fe–4S] cluster, and one [2Fe–2S] cluster comprise the bifurcating active site termed the electron-bifurcating flavobicluster (BF-FBC), which is found in all BfuABC family members. By using electron paramagnetic resonance spectroscopy, we identified spectral signatures originating from interactions between the FMN radical and [4Fe–4S]$^{+}$ cluster in the BF-FBC and observed temperature dependent behavior of the BF-FBC's [2Fe–2S]$^{+}$ cluster indicative of moderately slow spin–lattice relaxation. Additionally, we uncovered numerous spectral features corresponding to half-integer, $S > \frac{1}{2}$ spin states of [4Fe–4S]$^{+}$ clusters, including one attributable to the consequences of lysine-ligation of a [4Fe–4S] cluster unique to NfnABC. We contextualize these findings to electron transfer theory and NfnABC's structure. Our insights further the understanding of how enzymes are designed to exert control over electron transfer to conduct thermodynamically challenging reactions.

Received 5th December 2025,
Accepted 1st May 2026

DOI: 10.1039/d5dt02921j

rsc.li/dalton

1. Introduction

All forms of life rely on various energy transduction strategies for growth and survival. One energy transduction method is electron bifurcation (EB), whereby a single enzyme couples exergonic and endergonic oxidation–reduction (redox) reactions that are initiated by a common electron donor. This coupling provides a driving force for the endergonic process, thereby enabling the production of a high-value energy carrier in the cell *via* a net thermoneutral reaction.[1] The understanding and subsequent translation of EB principles to artificial systems could provide new avenues for powering thermodynamically challenging chemical processes. Frameworks for EB have emerged,[2] but further investigation into the physical properties of redox sites in EB enzymes are needed to elucidate the molecular principles that mediate EB function.[3–5] Here, we investigate such properties in an EB enzyme called NADH-dependent reduced-ferredoxin:NADP^{+} oxidoreductase (Nfn) to decipher aspects of electron tunnelling within its electron transfer (ET) relay.

Nfn enzymes contain iron–sulfur (Fe–S) clusters and flavin (FMN and/or FAD) cofactors that, under physiological conditions,[1] couple the exergonic reduction of NAD^{+} by NADPH to

[a]*Biosciences Center, National Laboratory of the Rockies, Golden, CO, 80401, USA. E-mail: cara.lubner@nlr.gov, gregory.vansuch@nlr.gov*
[b]*Department of Biochemistry & Molecular Biology, University of Georgia, Athens, GA, 30602, USA*

the endergonic reduction of ferredoxin (Fd_{ox}) by NADPH as described by eqn (1) †:

$$NAD^+ + 2NADPH + 2Fd_{ox} \leftrightarrow NADH + 2NADP^+ + 2Fd_{red} + H^+ \quad (1)$$

Two different versions of Nfn are known, those termed NfnSL,[6] ‡ and those termed NfnABC.[7] § Aside from catalyzing the same reaction, they have little in common and belong to different EB enzyme families: NfnSL enzymes belong to their own family aptly named NfnSL and NfnABC enzymes are members of the BfuABC family.[8]

NfnSL is a rare example of an EB enzyme with a relatively well-established mechanistic framework, which is primarily based on structural information[9,10] complemented by electrochemical and spectroscopic studies.[3,5,10,11] Near the center of the enzyme, the NfnL subunit houses an FAD cofactor that is the site of electron bifurcation (BF-FAD). It oxidizes NADPH and sends the two electrons along distinct pathways, one consisting of a site-differentiated [2Fe–2S] cluster and a non-bifurcating FAD site within NfnS, and the other consisting of the site-differentiated [4Fe–4S] and canonical [4Fe–4S] clusters within NfnL (Fig. 1a; two rounds of NADPH oxidation occur). To generate reduced substrates, the non-bifurcating FAD reduces NAD^+ by two electrons *via* hydride transfer and the canonical [4Fe–4S] cluster in NfnL reduces Fd_{ox}.[9,10]

Prevailing hypotheses about how NfnABC conducts EB primarily derive from studies that demonstrated its structural framework is drastically different from NfnSL.[7,12–14] The ability to catalyze NADPH oxidation is integrated into conserved aspects of the BfuABC family, including placement of the catalytic site that oxidizes the electron donor at one edge of the enzyme (Fig. 1b).[12,15–17] The electrons harnessed by oxidation of the donor tunnel to the bifurcating flavobicluster (BF-FBC), which is comprised of an FMN (located in the B-subunit), a [4Fe–4S] cluster (termed B1,§ located in the B-subunit), and a [2Fe–2S] cluster (termed C1, located in the C-subunit).[13,14] The FMN has two main functions, (1) reducing NAD^+ and (2) sending two electrons along a conformationally mediated ET route that leads to the Fd_{ox} reduction site (Fig. 1b).[12–16,18]

The molecular underpinnings of long-range and conformationally mediated electron tunnelling in the BfuABC family remains enigmatic. Investigations of Fe–S cluster containing enzymes/proteins have indicated that factors such as the electronic coupling between cofactors,[3,19,20] the spin-state accessibility of a cluster,[3,21–23] and the vibrational properties of a cluster[24] are important to consider when deciphering discrete ET steps. There is currently no information about these properties within NfnABC, which we set out to uncover in the structurally and biochemically characterized NfnABC from *Thermococcus sibiricus*.[8,14]

Cryo-EM structures of *Tsi* NfnABC demonstrated the cofactor layout depicted in Fig. 1c. This layout and the overall enzyme structure can be parsed into three main components: (1) the NfnL-like domain in NfnA that contains an FAD, a [4Fe–4S] cluster termed A7 with a non-canonical lysine ligand, and a [4Fe–4S] cluster termed A6; (2) the remainder of NfnA; and (3) NfnB and NfnC. The latter two are highly conserved components of the BfuABC family.[8,25] In contrast, the NfnL-like domain is unique to NfnABC, and its FAD and A7 cofactors have evident similarities to their NfnL counterparts.[7,12–14] However, the FAD does not bifurcate electrons and its amino acid environment has notable differences to the BF-FAD in NfnL, including the lack of an arginine residue postulated to contribute to the bifurcating capability of the BF-FAD (Fig. S1).[5,26] Furthermore, the non-canonical ligand of the [4Fe–4S] cluster adjacent to the FAD is a lysine (K165, *Tsi* numbering¶) whereas it is a glutamate in NfnL (Fig. 1a, c and Fig. S1, Tables S4, S5).[12–14]

Curiously, the entire function of NfnABC depends on A7's non-canonical lysine ligand (Fig. 1c).[12,14] Mutation of the lysine to a glutamate in *Tsi* NfnABC (K165E), which made the cluster ligation identical to its NfnL counterpart, resulted in <0.5% EB activity *vs.* wild type (WT) enzyme.[14] Unravelling differences of A7's electronic structure in the WT enzyme *vs.* the K165E variant could inform on mechanistic ramification(s) of this biochemical finding, and we therefore included this variant in our study.

Here, we used continuous wave X-band electron paramagnetic resonance (CW X-band EPR) spectroscopy to study the properties of redox sites in WT and K165E *Tsi* NfnABC. Notably, we detected spin–spin coupling between the FMN flavosemiquinone and $[4Fe–4S]^+$ cluster within the BF-FBC and observed slow spin–lattice relaxation behavior of the $[2Fe–2S]^+$ cluster within the BF-FBC. Furthermore, we discovered half-integer, $S > \frac{1}{2}$ spin states of $[4Fe–4S]^+$ cluster(s), with one being linked to A7's lysine-ligation. These findings are contextualized to electron tunnelling within the BF-FBC and the NfnL-like domain.

2. Results and analysis

2.1 *Tsi* NfnABC reduced by sodium dithionite

CW X-band EPR spectra were collected on sodium dithionite (NaDT) reduced samples in magnetic field regions corres-

† Stoichiometries that use $1Fd_{ox}$ and $1Fd_{red}^{2-}$ are also found in the literature,[6–9,13] which correspond to cases where a Fd harbouring two [4Fe–4S] clusters were used in activity assays (the Fd presumably functions as a 2-electron donor/acceptor). Assays[8,14] and cryo-EM structures[14] pertaining to *Tsi* NfnABC utilized a Fd from *Pyrococcus furiosus* that contains a single [4Fe–4S] that is a one-electron donor/acceptor.

‡ NfnSL is also referred to in the literature as NfnAB.[1,6,8,9] Because it is the NfnB subunit of NfnAB that has homology to the A subunit of the BfuABC family member NfnABC, we elected to use the NfnSL nomenclature[10] to mitigate confusion.

§ The subunit nomenclatures and Fe–S cluster terminology in the BfuABC family are not always consistent between research groups. Tabulations of our nomenclature and that used by other groups are provided in Tables S1–S3 of the SI.

¶ Because the annotated sequence of *Tsi* NfnABC incorrectly contains 8 additional amino acid residues after the start codon, the amino acid numbering in pdb files labels this lysine as K173, although it is K165 (see Fig. S6 in ref. 14).

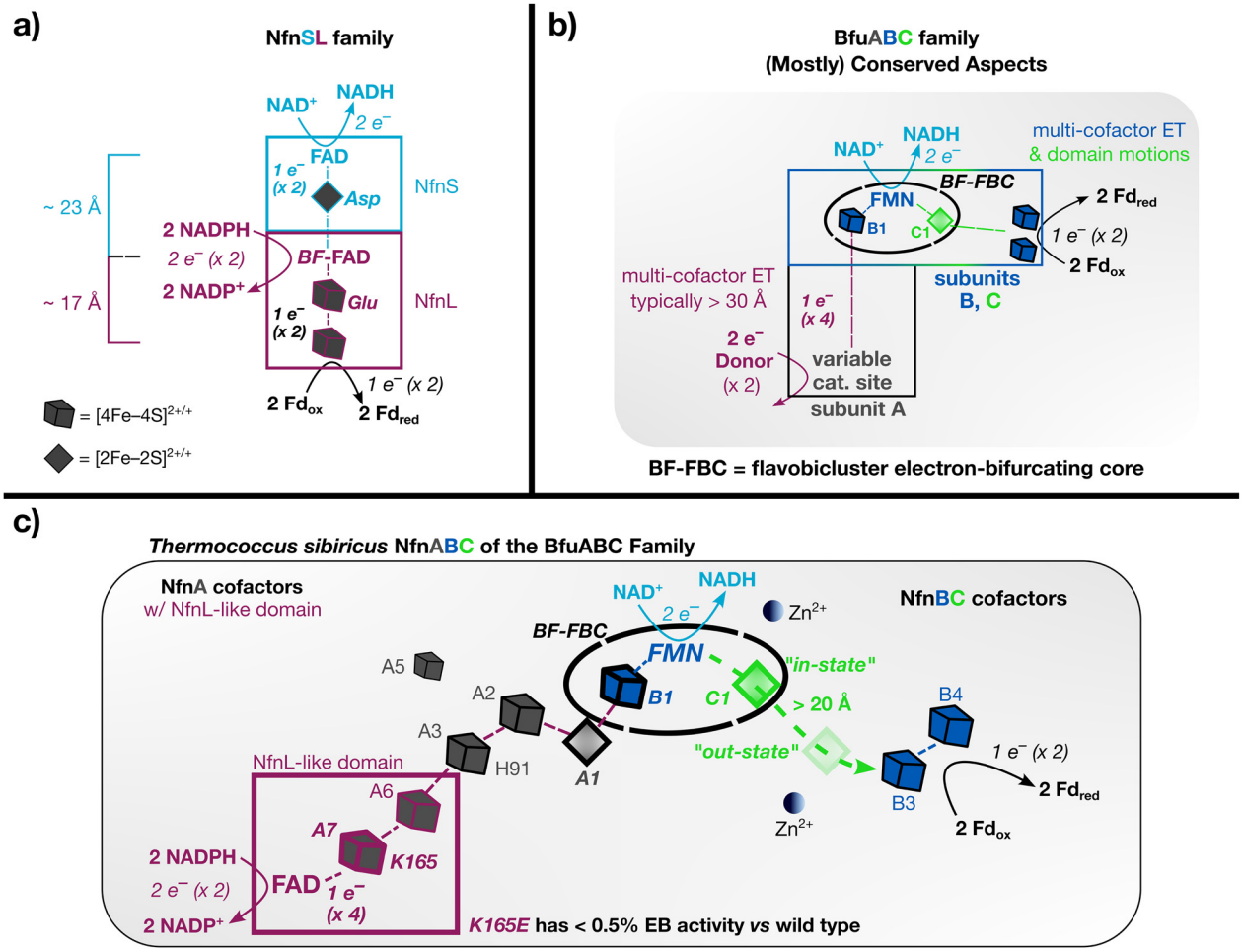

Fig. 1 (a) Depiction of the cofactor layout and ET routes in the NfnSL family of EB enzymes. (b) A simplified layout of the ET pathways in the BfuABC family. (c) Depiction of the cofactor layout in *Tsi* NfnABC, with an emphasis on cofactors that displayed discernible spectroscopic signatures in this study (A7, A1, B1, FMN, and C1). The site-differentiated A7 cluster has a lysine ligand (K165) and the site-differentiated A3 cluster has a histidine ligand (H91). The A1–A3 and A5 clusters are common to many A-subunits of BfuABC family members. The NfnB and NfnC subunits and their cofactor compositions are highly conserved in the B- and C-subunits, respectively, of all BfuABC family members.[8,25] Two locations of the C1 cluster are depicted, which arise from conformational changes facilitated by a flexible 11 amino acid linker between the C-terminal domain of NfnC, which harbors C1, and the more rigid N-terminal domain: there is the "in-state" (in which C1 is within ET distance of the FMN, bolded) and the "out-state" (in which C1 is within ET distance of B3, faded). Structures with Fd bound to *Tsi* NfnABC indicated one of the B3/B4 clusters reduces Fd_{ox}.[14] The A5 cluster is off pathway (>16 Å from A2) and has no discernible ET function.[14] For simplicity, arrows are drawn to depict the reaction in the NADPH oxidation direction for producing NADH and Fd_{red}. FAD = flavin adenine dinucleotide; FMN = riboflavin-5′-phosphate; $NADP^+$/NADPH, nicotinamide adenine dinucleotide phosphate (oxidized/reduced); NAD^+/NADH, nicotinamide adenine dinucleotide (oxidized/reduced). For visualization purposes, the additional H^+ dictated by the reaction stoichiometry of eqn (1) has not been included in this figure. During the EB mechanism, it is (reasonably) presumed that the [4Fe–4S] and [2Fe–2S] clusters accept/donate one electron at a time and cycle between the +2 (diamagnetic) and +1 (paramagnetic) redox states.

ponding to (1) $S = \frac{1}{2}$ signals (g ~2 region) and (2) $S > \frac{1}{2}$ signals and moderately strong spin–spin coupling interactions (low-field region). NaDT is a non-physiological reductant with a reduction potential (E') of −500 mV *vs.* SHE at pH 7.5 near ambient temperature.[27] Because of its moderately low E', it can "overload" a sample with reducing equivalents relative to higher-potential physiological reductants, which can help overcome anti-redox cooperativity effects that might otherwise prohibit spin–spin coupling observations.

2.1.1 Detection of a single $[2Fe–2S]^+$ cluster and spin–spin coupling between pair(s) of clusters. EPR spectra of NaDT-treated samples in the g ~2 region are displayed in Fig. 2a (T = 10 K) and Fig. 2b (T = 55 K). There was no evident flavosemiquinone signal near g ~2, so the signals originate from Fe–S clusters. Typically, g ~2 features from $[4Fe–4S]^+$ clusters are observable at $T \leq 40$ K, while those from $[2Fe–2S]^+$ clusters are observable above 40 K.[28] Because *Tsi* NfnABC houses ten clusters, the very low temperature spectra are incredibly complex; the spectral features could correspond to any of the Fe–S clusters and to spin–spin interactions between adjacent clusters.[28,29] Most of the signals broadened by 45 K, leaving behind a rhombic feature with g ~2.02, 1.94, 1.93, which are

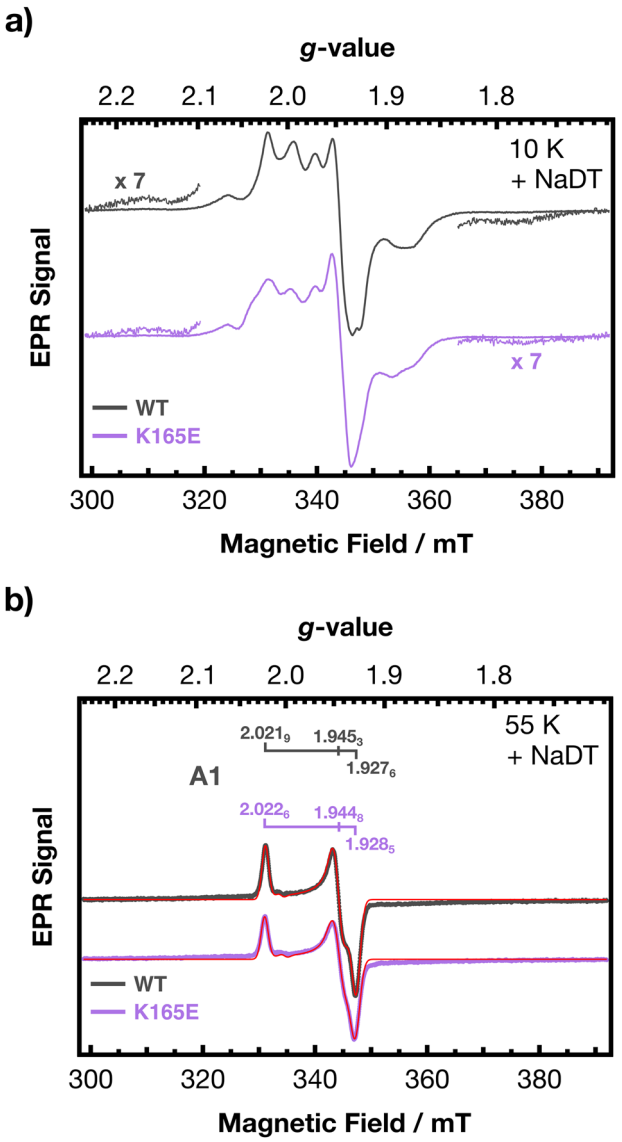

Fig. 2 EPR spectra of NaDT-treated samples in the g ~2 region at pH = 7.5. (a) Spectra at T = 10 K, which display complex signals arising from all reduced clusters and spin–spin coupling, the latter emphasized by the broad wing features magnified by ×7. Microwave power (P) = 10 μW. (b) Spectra and corresponding fits at T = 55 K (P = 100 μW). Modulation amplitude = 0.2 mT. Detailed temperature profiles are provided in Fig. S2 (WT) and S3 (K165E).

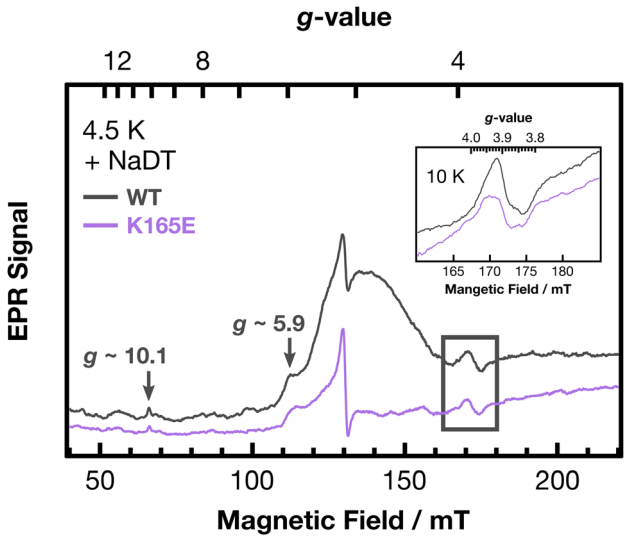

Fig. 3 Low-field EPR spectra of *Tsi* NfnABC at T = 4.5 K. The box emphasizes $\Delta|M_s| = 2$ transitions that originate from spin–spin coupling between pair(s) of adjacent Fe–S clusters. Inset: zoom-in of the $\Delta|M_s| = 2$ resonances at T = 10 K. Apparent differences between the WT and K165E $\Delta|M_s| = 2$ signals could be consequences of the K → E mutation.[3] P = 200 mW and modulation amplitude = 0.6 mT. The pH was 7.5. Detailed temperature profiles are provided in Fig. S14–S19 (WT) and S21–S26 (K165E).

similar values to those reported for $[2Fe–2S]^+$ A1 homologs.[22,30–32] This signal is accordingly assigned to A1 (Fig. 2b and Table S9).

There were two key pieces of evidence for spin–spin coupling, broad wing features in the g ~2 region (Fig. 2a) and $\Delta|M_s| = 2$ transitions near g ~3.89 and 3.83 (Fig. 3 and Fig. S19, S26).[29] These features originate from adjacent $S = \frac{1}{2}$ clusters that interact to form $S_{eff} = 0$ and 1 states, with zero-field splitting effects affording the observation of $\Delta|M_s| = 2$ transitions between the $|1\ -1\rangle$ and $|1\ 1\rangle$ energy levels.[33,34] Because of the close proximity between adjacent clusters along the ET pathway (often < 8 Å ‖) a general assignment of the coupling to specific pair(s) of clusters is not feasible. Nevertheless, we can use precedent to provide tentative assignments and constraints. First, we note that spin–spin coupling between B3 and B4 was reported in a truncated B-subunit of the BfuABC family member *Thermotoga maritima* hydrogenase HydABC (*Tma* HydABC)[32] and that an unassigned resonance reminiscent of a $\Delta|M_s| = 2$ transition was detected in holo-*Tma* HydABC.[35] Additionally, a $\Delta|M_s| = 2$ transition attributable to spin–spin coupling between A7 and A6 homologs was detected in an isolated NfnL subunit.[3,5] Therefore, the interactions detected in holo-*Tsi* NfnABC could stem from B3–B4 and A7–A6. Secondly, EPR studies of NfnA homologs in the hydrogenases from *Clostridium pasteurianum* (*Cp*I)[36] and *Clostridium acetobutylicum* (*Ca*I)[22] lacked $\Delta|M_s| = 2$ transitions. Thus, an origin of the $\Delta|M_s| = 2$ resonances being from adjacent clusters present in both *Tsi* NfnA and HydA1, A3/A2 and A2/A1 (Table S8), can be tentatively ruled out.[37] Lastly, equilibrium conformations at protein interfaces (*i.e.* subunit-subunit and flexible domain-domain interfaces) may be insufficient[38] for detectable interactions between surface exposed cofactors, therefore A6-A3 and A1-B1[12,14] coupling can be tentatively ruled out.

2.1.2 High-spin states. Low-field spectra of the NaDT-treated samples displayed half-integer, $S > \frac{1}{2}$ high-spin state resonances (Fig. 3 and 4a). Because the valence localized nature of $[2Fe–2S]^+$ clusters with pure cysteine-ligation like A1 and C1 makes their adoption of higher-spin states

‖ Based on Cys–Cys ligand distances (see also Fig. S1).

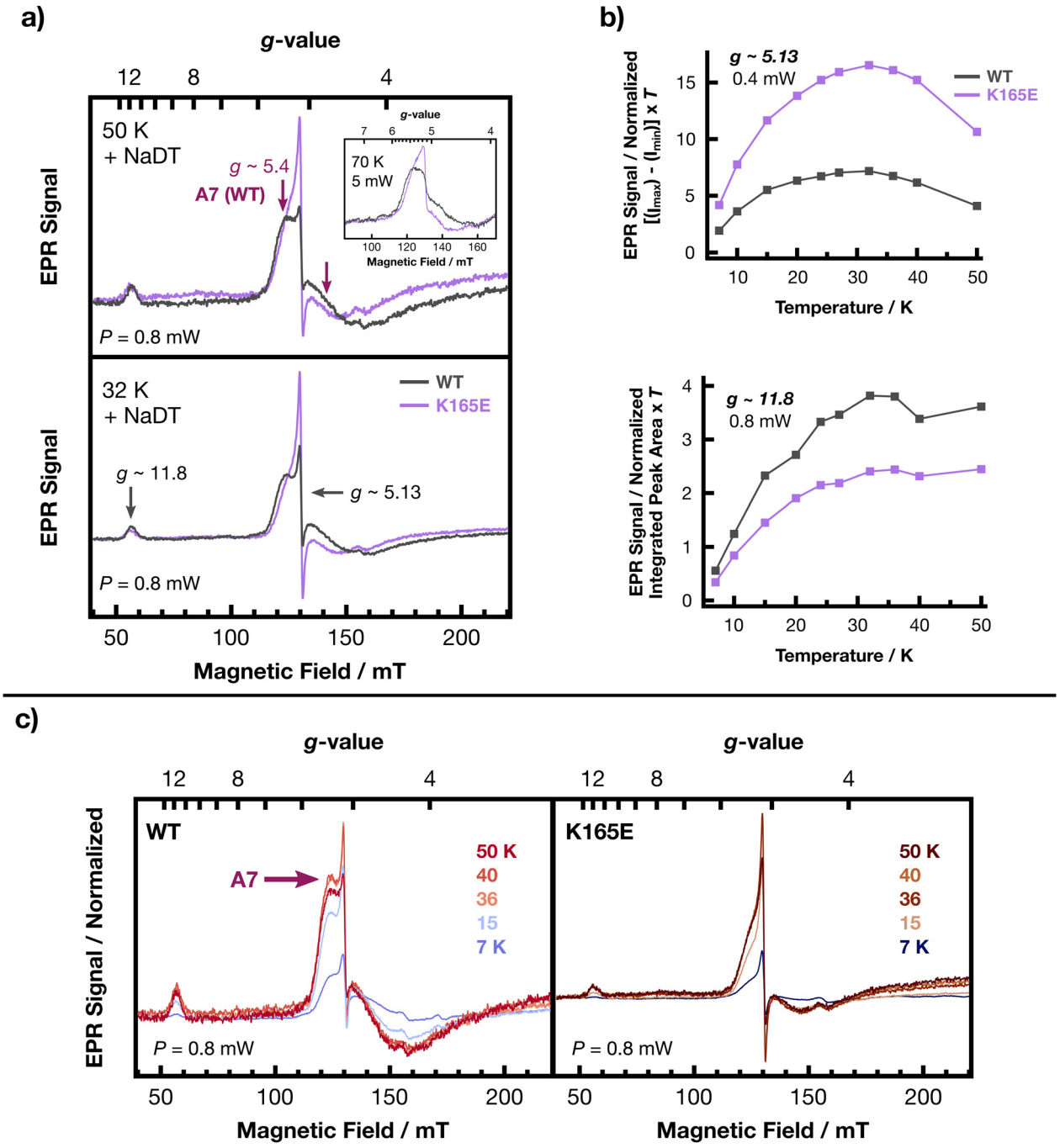

Fig. 4 (a) Higher-spin states signals of [4Fe–4S] clusters at pH = 7.5 of WT and K165E *Tsi* NfnABC at T = 32 and 50 K (P = 0.8 mW and modulation amplitude = 0.8 mT). The y-axis scale is not identical for the two plots. Power normalized spectra between T = 7–50 K at various microwave powers are provided in Fig. S8–S11 . For each temperature, the power normalized spectra were essentially identical, indicating a lack of power saturation up to at least 0.8 mW for each feature. Furthermore, the g ~5.1 peak-to-peak intensities (Tables S12 and S13) and the g ~11.8 peak areas (Tables S14 and S15) also demonstrated a lack of power saturation, with the normalized signal intensities (S) typically being within 5% of the expected values based on the relationship $S \propto \sqrt{P}$. Inset: Zoom-in of the g ~5.13 region of WT and K165E spectra at 70 K with P = 5 mW and modulation amplitude = 0.6 mT (see also Fig. S34 and S35). (b) Temperature normalized peak-to-peak intensity of the g ~5.13 feature plotted *vs.* temperature for P = 0.4 mW (top) and temperature normalized peak area of the g ~11.8 signal plotted *vs.* temperature at P = 0.8 mW (bottom). The g ~11.8 intensity was determined as the integrated peak area between 55 and 58.5 mT (after a baseline correction, Fig. S12 and S13). (c) Temperature normalized intensity of the WT (left) and K165E (right) enzyme low-field spectra for P = 0.8 mW at 7, 15, 36, 40, and 50 K. This panel emphasizes the excited state behavior of the g ~5.4 features, one being ascribed to the A7 cluster in WT enzyme. The y-axis scale is not identical for the two plots. The minor isotropic feature near g ~4.3 (~155 mT) in all spectra within panels (a) and (c) arises from adventitious Fe^{3+}.[34,41]

Table 1 Low-field EPR *g*-values of WT *Tsi* NfnABC and select NfnA(BC) homologs. Tentative cluster and spin-state assignments are provided (see also main text)

Enzyme/cluster	A7 (Lys-ligated)	A3 (His-ligated)	A3 (His-ligated)/A2	A3 (His-ligated)/A2/A6[a], B1/B3/B4	Source
Tsi NfnABC	5.4 (ES); S = 5/2 or 7/2 (?) Very broad	n.d.	5.9 (a, GS); S = 3/2	5.13 (d), 10.1 (a), 11.8 (a) (ES); S = 7/2	This work
Tma HydABC	n.a.	n.d.	5.7 (a, GS); S = 3/2	5.15 (d); $S \geq 5/2$ 5.55 (s); $S \geq 5/2$ 10.3 (a); S = 7/2 or 9/2	35
*Cp*I (HydA)	n.a.	n.d.	5.8 (a, GS); S = 3/2 4.76 (a, GS); S = 3/2	n.a.	36
*Ca*I (HydA)	n.a.	5.1 (d); S = 7/2 5.6 (s); S = 3/2	n.d.	n.a.	22

a = absorption, d = derivative, s = shoulder feature. GS = ground state; ES = thermally accessible excited state; n.a. = not applicable, n.d. = not detected. [a] *Tma* HydABC does not have an A6 homolog.

improbable,[39,40] we restrict assignments of the high-spin resonances to $[4Fe–4S]^+$ clusters.

The g ~5.9 resonance had an apparent positive absorption lineshape that was most pronounced between 4–7 K, above which it became shoulder-like prior to broadening beyond detection (Fig. S14–S18 and S21–S25). Rhombograms indicate the resonance originates from a transition within the $|\pm3/2\rangle$ Kramers doublet of an S = 3/2 ground state with an inverted spin multiplet (D < 0, with D = axial zero-field splitting parameter).[41] Similar resonances were reported for the NfnA(BC) homologs *Tma* HydABC[35] and *Cp*I,[36] so it may stem from a $[4Fe–4S]^+$ cluster common to all three enzymes: A3 or A2 (Table 1 and Tables S2, S8).[14,17,37]

The g ~5.13 resonance was the most pronounced low-field feature in both WT and K165E spectra (Fig. 3 and 4a). Under non-saturating conditions, its normalized peak-to-peak amplitude increased concomitantly with temperature until ~32 K (Fig. 4b, top), which is indicative of a thermally accessible excited state.[42] The strong intensity and isotropic lineshape of the resonance indicate it is best described by the point of "mathematical coincidence" on a rhombogram, where all three g-values are equivalent. For a g ~5.13 signal, this corresponds to the $|\pm3/2\rangle$ doublet of an S = 7/2 system with the rhombic (E) and axial (D) zero-field splitting parameter ratio being ~0.117.[34,41]

Additional low-field resonances observed in WT and K165E spectra were g ~10.1 (Fig. 3) and 11.8 ** (Fig. 4a). The weak intensity of the g ~10.1 resonance precluded a reliable temperature-based analysis under non-saturating conditions. Nonetheless, it was observed up to ~32 K (Fig. S20 and S27). The temperature profile of the stronger g ~11.8 signal under non-saturating conditions demonstrated a concomitant increase of signal intensity with temperature until ~32 K, above which the intensity persisted until at least 50 K (Fig. 4b, bottom). This indicates the g ~11.8 signal corresponds to a thermally accessible excited spin state.[42]

Reports of similar g ~12 signals are rare, and such signals are accompanied by an isotropic g ~5.1 resonance with E/D ~0.117.[43–45] We already assigned a g ~5.13 resonance to the excited $|\pm3/2\rangle$ doublet of an S = 7/2 system with E/D ~0.117, and rhombograms indicate the g ~10.1 feature aligns well for a transition within the $|\pm5/2\rangle$ doublet of an S = 7/2 system with E/D ~0.117 and that the g ~11.8 feature aligns well for a transition within the $|\pm1/2\rangle$ doublet of an S = 7/2 system with E/D ~0.117. Therefore, the evidence points to the g ~5.13, 10.1, and 11.8 resonances originating from different excited Kramers doublets of the same S = 7/2 system. The temperature profiles (loss of the g ~10.1, attenuation of the g ~5.13, and persistence of the g ~11.8 intensity) implicate an inverted spin multiplet (D < 0).[41,42] ** This analysis agrees with previous reports of S = 7/2 $[4Fe–4S(Se)]^+$ clusters.[44–46] ††

Because resonances at g ~5.1 and 10.3 were reported for holo-*Tma* HydABC,[35] the S = 7/2 system could correspond to a $[4Fe–4S]^+$ cluster common to *Tsi* NfnABC and *Tma* HydABC: A3, A2, B1, B3 or B4 (Table S2, S3).[8,14,17] We also cannot rule out a possibility the spin system belongs to A6 due to its atypical cysteine motif (Table 1 and Fig. S1, Table S5, further addressed in the Discussion).

The pronounced g ~5.4 resonance in the WT spectra is ascribed to the lysine-ligated A7 cluster, an assignment well supported by the altered lineshape and temperature profile in K165E spectra (Fig. 3, 4a and Fig. S15–S17, S22–S24, S34, S35). Additional comparison to K165E indicates that much of the broad signal between ~125 to 150 mT is a constituent of the WT g ~5.4 feature. Under non-saturating conditions, normalized WT spectra demonstrated the g ~5.4 signal increases with temperature until ~40 K, indicative of a thermally accessible excited spin state (Fig. 4c).[42]

** The possibility of the g ~11.8 feature originating from S = 2 $[3Fe–4S]^0$ cluster(s) was ruled out with parallel mode EPR spectroscopy (Fig. S36).

†† We have provided what we find is the most reasonable conclusion based on our data and literature precedence.[44–46] We cannot rule out a possibility that the g ~10.1 resonances corresponds to the $|\pm5/2\rangle$, $|\pm3/2\rangle$, or $|\pm1/2\rangle$ Kramers doublet of an S = 9/2 system (based on rhomobogram rules, detecting a g ~10 signal within $|\pm1/2\rangle$ Kramers doublet of an S = 9/2 system is unlikely).[41] We also cannot rule out a possibility that the g ~11.8 signal originates from the $|\pm3/2\rangle$ doublet of an S = 9/2 cluster.[41]

Assigning A7's low-field resonance to a particular spin state is not intuitive. This is primarily because of its breadth, which is attributable to *D*-strain.[47] Given the strong intensity of the resonance, we assume its shape is best described by a broad *E*/*D* distribution that is skewed about a point of "mathematical coincidence" on a rhombogram (for $S > 3/2$) or that is approaching maximal rhombicity (for $S = 3/2$).[34,47] Within this framework, the abrupt decline of signal intensity between $g \sim 5.4$ to 6 makes the $|\pm 3/2\rangle$ doublet of an $S = 9/2$ system difficult to rationalize and the lineshape and *g*-value range of the signal makes an $S = 3/2$ spin system unlikely. This means an origin from the excited $|\pm 3/2\rangle$ doublet of an $S = 5/2$ or 7/2 system is the most likely scenario (Table 1), the latter requiring *E*/*D* to not exceed a value of ~0.17.[41] We cannot rule out a possibility that this resonance is inapplicable to a rhombogram analysis.

Spectra of the K165E variant exhibited a different $g \sim 5.4$ resonance with a temperature profile indicative of an excited state (Fig. 4c). The strong intensity and apparent positive absorption lineshape corresponds best to an $S = 3/2$ state.[41] We cannot reliably ascribe this signal to a particular cluster. It could correspond to a different high-spin state of A7 caused by the K → E mutation. But it cannot be ruled out that the signal corresponds to a different cluster entirely, with its presence masked in WT enzyme. Indeed, studies of the A3-homolog from *Ca*I[22] and the A3-containing *Tma* HydABC[35] reported a similar resonance.

The $g \sim 5.13$ signal intensity was stronger in the K165E spectra (Fig. 3 and 4a). This observation is difficult to rationalize, and we offer two explanations. One rationale is that the K → E mutation alters the electronic structure of A7 such that it adopts an excited state manifest by a $g \sim 5.13$ signal. In support of this rationale, we note that the glutamate-ligated A7 homolog in NfnL exhibits a sharp $g \sim 5.1$ signal.[3] A second possibility is that the K → E mutation perturbs the protein structure,[48] which could alter nearby Fe–S cluster electronic structures[23] and generate additional excited spin state populations manifest by a $g \sim 5.13$ signal. Regardless, the strong intensity and isotropic nature of the additional $g \sim 5.1$ signal infers it originates from the $|\pm 3/2\rangle$ doublet of an $S = 7/2$ system.[41]

Overall, the spectra of NaDT reduced WT and K165E samples provided a wealth of information about the electronic properties of Fe–S clusters in *Tsi* NfnABC. However, NaDT-treatment did not allow for the detection of any paramagnetic flavosemiquinone ($S = \frac{1}{2}$) features, probably because the low reduction potential of NaDT causes the FAD and FMN sites to be fully reduced to the EPR silent flavohydroquinone form ($S = 0$). We hypothesized this could be mitigated by using the higher-potential, biologically relevant reductants NAD(P)H.[1] On a similar note, measurements with NaDT-treated samples did not inform on the equilibrium distribution of paramagnetic species generated under physiological-like conditions, which is needed for understanding ET under biological-like conditions and for reinforcing the biological relevance of uncommon findings from NaDT-treatment, namely the observation of excited states (Fig. 4). Thus, we turned to the use of NAD(P)H as reductants.

2.2 *Tsi* NfnABC reduced by NAD(P)H

EPR spectra were collected on samples reduced by the 2-electron donor NAD(P)H. We hypothesized the resultant equilibrium distribution of electrons would be perturbed by the presence of the complementary electron acceptor, $NAD(P)^+$ (eqn (1)). Thus, samples treated with both the reductant and complementary oxidant were examined as well.

We attempted to oxidize WT enzyme with various dyes (thionine, 2,6-dichlorophenolindophenol, and phenazine methosulfate) to obtain an EPR silent baseline spectrum, meaning the flavins and clusters would be oxidized, EPR inactive $S = 0$ species. Unexpectedly, this was not successful. Numerous paramagnetic species were still observed, including that of A1, various $S = \frac{1}{2}$ resonances of $[4Fe\text{–}4S]^+$ cluster(s), and $S > \frac{1}{2}$ signals (see Fig. S4 for example spectra). However, the as-isolated K165E sample was essentially EPR silent, enabling us to use K165E data to monitor paramagnetic species generation beginning with an EPR silent "zero point".

2.2.1 Evidence for a flavosemiquinone at the FMN site and spin–spin coupling between the FMN site and the reduced B1 cluster within the BF-FBC. Fig. 5a shows $T = 200$ K EPR spectra in the $g \sim 2$ region of NAD(P)H-treated WT enzyme, with spectra from "oxidized" and NaDT-treated samples included for comparison. Strong radical features were detected in the NAD(H)-treated samples. The linewidth of the radical (as measured at $P = 1$ mW with the NADPH + NAD^+-treated and NADH-treated samples) was ~2.1 mT, which is diagnostic of a neutral flavosemiquinone (Fig. S5).[5,49] Because (i) observation of the flavosemiquinone required NAD(H), which binds at the FMN site,[12,14] and (ii) a FMN-flavosemiquinone was reported for *Tma* HydABC[50] and for the NfnBC homolog of the non-bifurcating formate dehydrogenase from *Cupriavidus necator* (formerly *Ralstonia eutropha*, *Cn* FdsBG)[51] under similar conditions, we ascribe the observed flavosemiquinone in *Tsi* NfnABC to the FMN site of the BF-FBC (Fig. 5a; see also Discussion a in the SI).

Coincident with the detection of the FMN-flavosemiquinone were signals near $g \sim 4$ that are consistent with $\Delta|M_s| = 2$ transitions arising from spin–spin interactions between the FMN-flavosemiquinone and a nearby $S = \frac{1}{2}$ Fe–S cluster.[52] Because of the close proximity of the FMN site and B1 (< 7 Å),[14] we assign this interaction to coupling between the FMN-flavosemiquinone and the $[4Fe\text{–}4S]^+$ B1 cluster of the BF-FBC (Fig. 5b; see also Discussion b in the SI).

2.2.2 Electron loading in the K165E variant upon NAD(P)H-treatment. Fig. 6a displays the $T = 10$ K EPR spectra in the $g \sim 2$ region for as-isolated K165E *Tsi* NfnABC as well as NADPH-, NADH-, and NADPH + NAD^+-treated samples. Each spectrum of NAD(P)H-treated samples displayed $S = \frac{1}{2}$ Fe–S signals and the NAD(H)-containing samples also exhibited a (probably saturated) derivative feature near $g \sim 2$ corresponding to the FMN-flavosemiquinone (see also Fig. S7). Furthermore, NAD(H)-treated samples exhibited the $\Delta|M_s| = 2$ transitions at $g \sim 4$ ascribed to coupling between the FMN-flavosemiquinone and B1 cluster (Fig. 6b). We did not detect broad wing features in

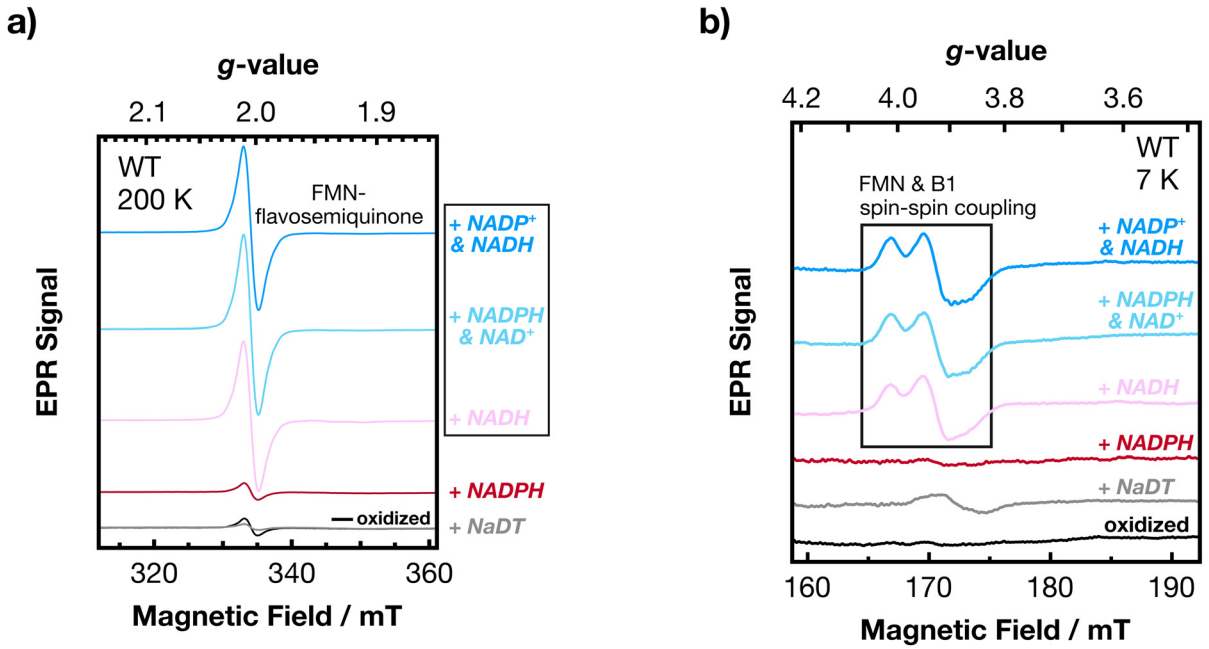

Fig. 5 (a) The g ~2 region EPR spectra at T = 200 K of WT samples treated with NAD(P)(H) at pH 7.5. The oxidized and NaDT reduced spectra are included for comparison. As described in the text, we assign the strong radical signal to the FMN site in the NfnB subunit. P = 16 mW, modulation amplitude = 0.5 mT. (b) Low-field spectra focusing on the g ~4 region at T = 7 K (P = 160 mW, modulation amplitude = 0.7 mT). The box highlights the $\Delta|M_s| = 2$ transitions ascribed to spin–spin coupling between the FMN-flavosemiquinone and B1 cluster.

the g ~2 region that are indicative of spin–spin interactions between adjacent Fe–S sites (Fig. 6a *vs.* Fig. 2a, ×7 traces).[29]

No high-spin signals were detected in as-isolated K165E *Tsi* NfnABC. Upon NAD(P)H-treatment, we could not reliably observe the S = 3/2 ground state signal at g ~5.9 detected in the NaDT-treated sample (Fig. S28). However, excited spin states were detected at g ~5.13, 5.4, 10.1, and 11.8 in the NAD(P)(H)-treated samples (Fig. 6b; spectra at T = 55 K are provided in Fig. S29 and a full temperature profile for the NADPH + NAD^+- treated sample in Fig. S30–S33). Thus, the equilibrium distribution of excited spin states observed in NaDT-treated K165E (the vast majority of which are observable in WT enzyme) were also detected under biological-like conditions.

At T = 55 K, each NAD(P)H-treated K165E sample contained a rhombic species attributable to the A1 $[2Fe–2S]^+$ cluster (g ~2.020, 1.945, and 1.928; Fig. 6c, Table 2, and Table S9). In addition to the A1 signals, the T = 55 K spectra of the NADH- and NADPH + NAD^+-treated samples displayed a strong isotropic derivative feature corresponding to the FMN-flavosemiquinone (g ~2.003) and an additional rhombic species, g ~2.007, 1.947, 1.913, that we assign to the C1 $[2Fe–2S]^+$ cluster (Fig. 6c, Table 2 and Table S10; the g_z component is masked by the FMN-flavosemiquinone).[30,32,51] The C1 signals were observable up to at least 200 K in K165E and WT enzyme (Fig. 6d and Fig. S37).

Spectra of WT enzyme prepared under turnover conditions (20× excess of NADPH, NAD^+, and Fd_{ox}) exhibited the FMN-flavosemiquinone and FMN-B1 coupling signals without detectable C1 signals (Fig. S38). Therefore, the observation of the FMN radical and its coupling with B1 do not ensure C1 detection.

Overall, because as-isolated K165E *Tsi* NfnABC was essentially EPR silent, the NAD(P)H-treatments afforded us the ability to detect the equilibrium populations of paramagnetic species derived solely from NAD(P)H oxidation. Reduction by NADPH demonstrated that electrons derived from NADPH transfer from the FAD site to at least the A1 cluster. NADPH + NAD^+- and NADH-treatment enabled the detection of C1. Despite its abolished EB activity,[14] K165E *Tsi* NfnABC remains ET competent. A rationalization for the lack of EB activity might involve differences of A7's higher-spin state but warrants further study.

2.3 Additional analysis of the g ~2 region

2.3.1 The B1 $[4Fe–4S]^+$ cluster. There are evident similarities within the g ~2 region among various spectra, especially from those collected with NAD(P)(H)-treated samples (Fig. 6a and Fig. S4, S6, S7). Because the NADPH + NAD^+- and NADH-treated samples should have an $S = \frac{1}{2}$ B1 signal (as exemplified by the $\Delta|M_s| = 2$ signals in Fig. 5b, 6b and Fig. S4, S30), tentative g-value assignments to B1 are possible. We assign the common features marked in the T = 20 K spectra shown in Fig. 7 to B1 (g ~2.038, 1.943, 1.894; see also Table 2). These values (and the general lineshape of these features) are similar to what was reported for the B1 homolog in *Cn* FdsBG[31,51] and are somewhat similar to the values reported for the B1 homolog in the isolated B-subunit from *Tma* HydABC (see also Table S11).[32]

2.3.2 Ambiguity of the remaining g ~2 resonances. An inevitable consequence of the cofactor complexity in *Tsi* NfnABC

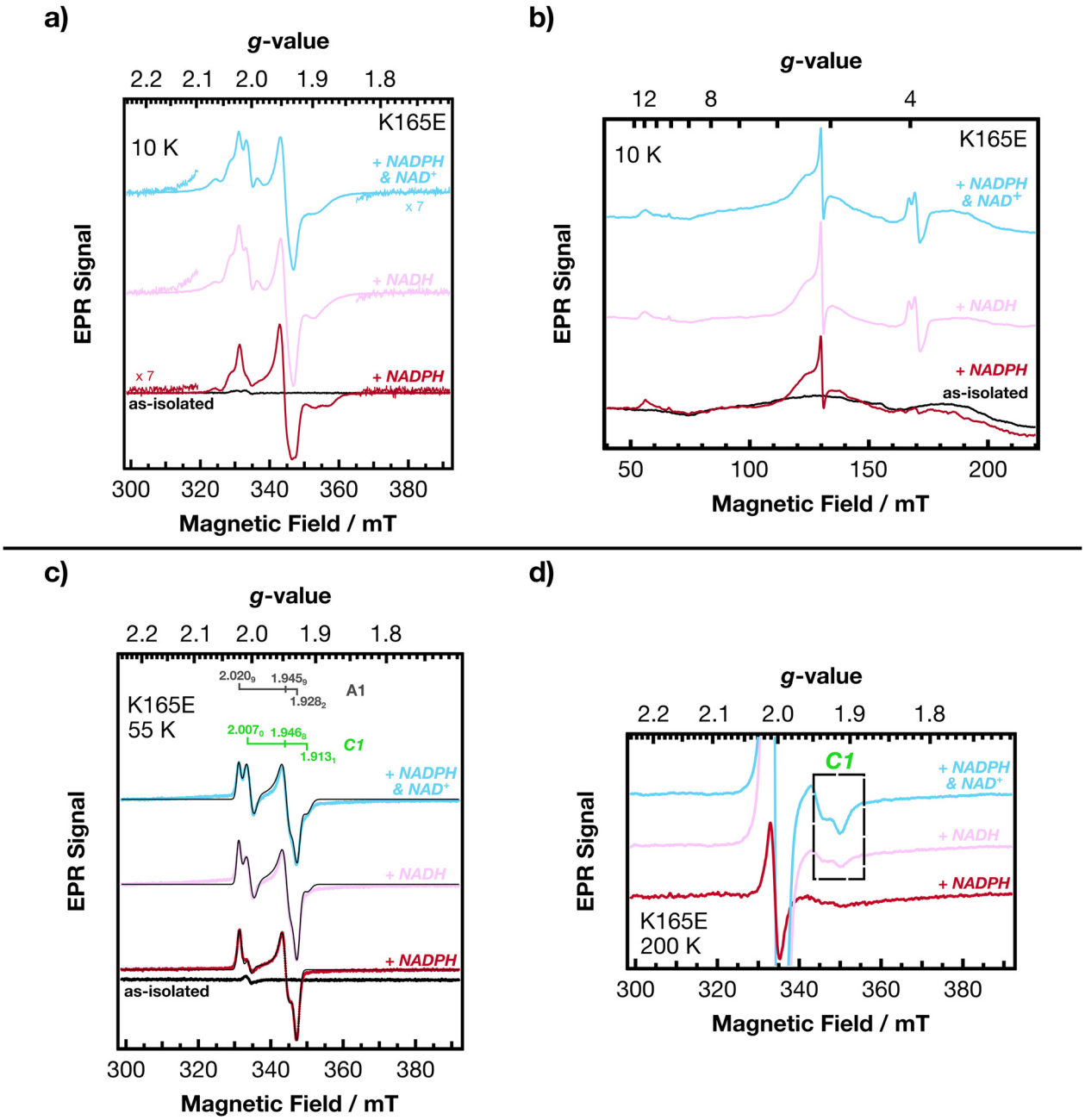

Fig. 6 (a) X-Band EPR spectra at T = 10 K in the g ~2 region of NADPH-, NADH-, and NADPH + NAD^+-treated K165E samples (pH 7.5). A spectrum of as-isolated K165E is shown for comparison and indicates that K165E *Tsi* NfnABC is essentially EPR silent prior to reductive treatment. Like in Fig. 2, the "wings" are emphasized with × 7 magnification, but unlike in Fig. 2 no broad wing features were observed. P = 10 μW, modulation amplitude = 0.2 mT. Temperature profiles for the NADPH- and NADPH + NAD^+-treated samples (collected on different days than the spectra displayed here) are provided in Fig. S6 and S7, respectively. (b) Corresponding low-field spectra at T = 10 K and P = 200 mW (modulation amplitude = 0.6 mT). (c) X-Band EPR spectra at T = 55 K in the g ~2 region of the NADPH-, NADH-, and NADPH + NAD^+- K165E samples. Spectral fits (thin black traces) are plotted on top of the data points. The NADPH-treated sample only exhibited signals from the A1 cluster, whereas the NADH- and NADPH + NAD^+-treated samples also contained signals from the C1 cluster and the FMN-flavosemiquinone (the latter with g ~2.003); see also Tables S9 and S10. Shown at the top of the graph are the g-values for the A1 cluster (obtained from the fit to the + NADPH spectrum) and the for the C1 cluster (obtained from the fit to the + NADPH & NAD^+ spectrum). P = 100 μW, modulation amplitude = 0.2 mT. (d) Representative T = 200 K spectra of NAD(P)H-treated K165E samples highlighting the C1 signals obtained from the NADH-treated and NADPH + NAD^+-treated samples. P = 50 mW and modulation amplitude = 0.2 mT.

is that g ~2 resonances remain unassigned. Given the broadness of A7's low-field feature (Fig. 3, 4a and c), it is feasible any $S = \frac{1}{2}$ resonances from this cluster are also broad. Notably, the g ~2.02–2.03 region is less well-defined in WT *vs.* K165E spectra (Fig. 2a, 7 and Fig. S2–S4, S6, S7, S39). This suggests additional cluster(s) contribute to this resonance in WT enzyme, with A7 being a probable candidate. Any additional A7 signal would presumably span from g ~2.03 to at least *ca.* g ~1.93–1.95. Provided

Table 2 EPR signal assignments in the g ~2 region for A1, C1, and B1

Cluster	Approx. g-values	Key figures (+ conditions for A1/C1)
A1	2.02, 1.94, 1.93	Fig. 2b (+NaDT) Fig. 6c (+NADPH, +NADPH + NAD^+; +NADPH + NAD^+)
C1	2.00, 1.95, 1.91	Fig. 6c (+NADPH + NAD^+; +NADPH + NAD^+) Fig. 6d (+NADPH + NAD^+; +NADPH + NAD^+)
B1	2.04, 1.94, 1.89	Fig. 7

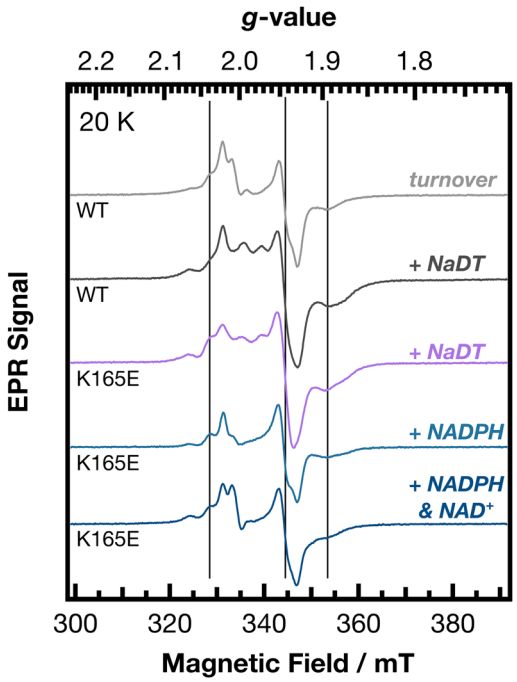

Fig. 7 Various WT and K165E spectra in the g ~2 region at T = 20 K. The vertical markers indicate common signals that we ascribe to B1 (Table 2). The g ~1.94 derivative component of B1 overlaps with the derivative component of the other Fe–S signals present in a given spectrum. P = 20 μW and modulation amplitude = 0.2 mT. The pH was 7.5. Additional WT turnover spectra are provided in Fig. S38.

a generalization with the Glu-ligated A7 homolog of NfnL is valid, A7 signals in the K165E variant would be constrained to the spectrally congested g ~2 to 1.93 region.[3,5]

Two notable unassigned resonances are those at g ~2.06 and 1.87 (Fig. 2a, 6a, 7 and Fig. S2–S4, S6, S7). Based on precedence, they may correspond to the histidine-ligated A3[22] or B3/B4.[32] To our knowledge, B3/B4 signals have only been identified in a truncated form of the *Tma* HydB subunit.[32]

3. Discussion

By placing our results in a nonadiabatic ET framework, we glean insight into the molecular control of cofactor function. The rate of ET (k_{ET}) between a donor cofactor (D) and acceptor cofactor (A) is described by eqn (2):[53,54]

$$k_{ET} = \frac{2\pi}{\hbar\sqrt{4\pi\lambda k_B T}} H_{DA}{}^2 e^{\frac{-(\Delta G^\circ + \lambda)^2}{4\lambda k_B T}} \quad (2)$$

where $\hbar$ is the reduced Planck's constant and k_B is the Boltzmann constant. For a given temperature (T), k_{ET} depends on the reorganization energy (λ), the driving force (ΔG°), and the electronic coupling (H_{DA}; or the qualitatively similar parameter T_{DA}). The latter is further described by eqn (3):

$$H_{DA} = H^0_{DA} e^{-\frac{\beta}{2}(r_{DA} - r_0)} \quad (3)$$

where H^0_{DA} is the close contact electronic coupling, r_0 is the close contact distance, r_{DA} is the D–A distance, and β is a decay factor that is influenced by r_{DA}, donor–acceptor orientation effects on the electronic coupling, and protein medium effects on the electronic coupling.[53,54]

The best studied EB enzymes from a mechanistic standpoint, *e.g.* cytochrome bc_1 and NfnSL, have extreme ΔG° gradients that explain k_{ET},[2,11] but steep energy landscapes may not apply to all EB enzymes. For example, the long-range and conformationally mediated ET employed by NfnABC may require an interplay of ΔG° and other parameters of eqn (2) for the efficient partitioning and control of electron transport, of which our data provide insight.

3.1 Spin–spin coupling ramifications on the β component of ET

Part of the exchange parameter of spin–spin coupling is a component of electronic coupling (*i.e.* H_{DA}).[55] Consequently, the $\Delta|M_s| = 2$ transitions ascribed to FMN-B1 (Fig. 5b) and tentatively A7-A6 and/or B3-B4 (see Section 2.1.1) are indicative of a moderately strong electronic coupling strength between these cofactors compared to what would be a weaker coupling strength if such features were attenuated at a comparable r_{DA}.[20,52] The close proximity of FMN-B1, A7–A6, and B3–B4 ($\leq$ 8 Å)[14] infers substantial through-space electronic coupling. The magnitude of this coupling, manifest by β, will be impacted by the donor–acceptor orientations.[53] The mechanistic ramifications are that the geometric orientations of certain cofactors in *Tsi* NfnABC exert control over β and therefore k_{ET}, specifically between the NAD^+ reduction site (FMN) and the closest electron donor (B1) of the BF-FBC, between A7 and A6 within the NfnL-like domain, and/or between B3 and B4 near the site of substrate Fd binding (Fig. 1c).

3.2 Slow temperature relaxation of C1 implicates ΔG° and /or λ control over ET in the BF-FBC

The two $[2Fe–2S]^+$ clusters had different temperature relaxation properties, with the A1 signals broadening beyond detection by ~125 K (Fig. S2, S3, S6, S7) and with C1 signals persisting until at least 200 K (Fig. 6d and Fig. S7, S37). Similar observations were made regarding NfnA and NfnC homologs in a hydrogenase from *Solidesulfovibrio fructosivorans* (*Sf* HndABCD, formerly *Desulfovibrio fructosovorans*)[30] and the

C1 homolog in *Cn* FdsBG.[51] Our study is the first to demonstrate the differential temperature relaxation behavior of A1 and C1 within a holoenzyme from the BfuABC family.

Temperature relaxation is often described by the spin–lattice relaxation time, T_1. The C1 cluster has a $CX_4CX_{35}CX_3C$ motif,[14] and clusters with this motif are known to have slower spin–lattice relaxation times (and therefore have resonances that persist to higher temperature) than $[2Fe–2S]^+$ clusters with motifs similar to that of A1 ($CX_{10}CX_2CX_{11}C$‡‡).[30] The differential spin–lattice relaxation properties of A1 and C1 means they qualitatively have different vibrational modes[56] that may dictate their reactivity, with ramifications regarding the λ (ref. 57 and 58) and $\Delta G°$ (ref. 24 and 59) terms of eqn (2). It is interesting to consider the dynamic protein interface/solvent exposure changes experienced by C1 during catalysis as the consequence of large-scale conformational changes of NfnC,[13,14] and that vibrational control over λ and/or $\Delta G°$ may contribute to the proposed,[32] albeit experimentally elusive, importance of C1 properties being modulated during the EB reaction.

3.3 Higher-spin states may exert control over ET steps at operative temperatures

The temperature dependence of spin-ladders renders ambiguity as to which higher-spin states are accessible at operative temperatures (>293 K).[60,61] Therefore, the data imply that under the experimental conditions, thermally accessible high-spin state electronic configurations of certain $[4Fe–4S]^+$ clusters become increasingly populated as the temperature increases *vs* their ground state electronic configuration. This implies that some $[4Fe–4S]^+$ cluster(s) in *Tsi* NfnABC have $S > \frac{1}{2}$ ET-active electronic configurations, inferring a mechanistic relevance of excited high-spin states at temperatures where *Tsi* NfnABC operates ($T > 350$ K (ref. 8 and 14)).[40]

Precise role(s) of high-spin Fe–S clusters within ET relays are largely unestablished from an experimental standpoint, although theoretical investigations suggest they can significantly influence the potential energy surface of an ET step,[62] namely *via* $\Delta G°$ and/or H_{DA} modulations.[63,64] By considering specific structural aspects of *Tsi* NfnABC in the next subsection, we realize (i) that the $S = 7/2$ state may correspond to ET steps regulated by the A3 or A6 clusters and (ii) that there are further mechanistic ramifications to consider regarding A7's high-spin state upon ET within the NfnL-like domain.

3.4 Contextualization to structural considerations regarding the His-ligated A3 cluster and the NfnL-like domain

The NfnL-like domain of *Tsi* NfnA is essentially a separate structural component, with the surface exposed A6 [4Fe–4S] cluster of the NfnL-like domain electronically connected to the surface exposed His-ligated A3 [4Fe–4S] cluster that is part of the remainder of NfnA.[12–14] The A3 and A6 clusters have unusual cysteine spacings that differentiate A3 from its homologs[25] and A6 from its NfnL homologs (Fig. 8 and Tables S5, S6). Directly relevant to the data herein, the surface exposure and/or unusual cysteine ligand spacing could promote higher-spin state accessibility. Specifically, structural flexibility in the region connecting the NfnL-like domain and the remainder of NfnA[12–14] could promote structural distortions that modify the properties of the A3 and/or A6 clusters, *i.e.* spin state accessibility.[65] A similar situation may occur in nitrogenase iron-proteins,[23,66] which contain a surface exposed [4Fe–4S] cluster with an atypical cysteine motif,[67] suggesting conformational control of spin states may not be uncommon in some complex metalloenzymes.

It is therefore probable that the $S = 7/2$ feature, underscored by the g ~5.13, 10.1, and 11.8 resonances (Fig. 3, 4 and Table 1), belongs to A3 or A6. Circumstantial evidence supports A3, as a study of the His-ligated cluster in *Ca*I detected a strong g ~5.1 resonance (but not a g ~10 or 11.8 resonance) with a similar temperature profile to the $S = 7/2$ feature in *Tsi* NfnABC,[22] and a study of A3-containing *Tma* HydABC detected g ~5.1 and 10 resonances (but not a g ~11.8 resonance). Although the temperature range studied for *Tma* HydABC was limited, the two resonances had similar temperature profiles to the analogous $S = 7/2$ features reported herein.[35] The differences between the observed resonances among the three enzymes could be related to the fact the cysteine motif and interfacial environment of the His-ligated cluster in *Tsi* NfnABC is drastically different from *Ca*I and *Tma* HydABC. The same motif and interfacial environment arguments hold for A6, making a tentative assignment of the $S = 7/2$ signal to A3 or to A6 equally reasonable.

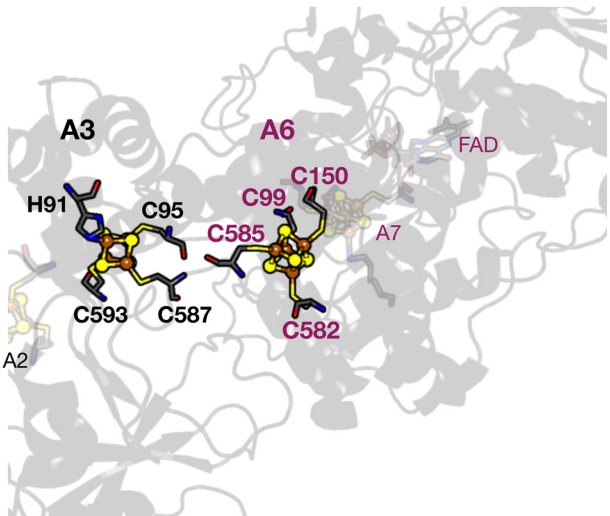

Fig. 8 A highlight of the region containing the A6 and His-ligated A3 clusters within the A subunit of *Tsi* NfnABC (pdb code 9N5U). The amino acid binding motif of A3 in NfnABC enzymes differentiates it from the homologous cluster in other BfuABC enzymes and non-bifurcating counterparts (Table S6) and the amino acid binding motif of A6 differentiates it from its NfnL counterpart (Fig. S1 and Table S5).

‡‡See also Uniprot ID C6A4M3 (for *Tsi* NfnA) and pdb code 9N5U.

Perhaps one of the most fascinating coordination chemistry aspects of NfnABC is the lysine ligation to A7 within the NfnL-like domain. Non-cysteine ligands are not uncommon for biological Fe–S clusters, but we are not aware of Fe–S clusters with a lysine ligand other than A7 in NfnABC. It has been reasonably hypothesized that the lysine imparts atypical properties upon the A7 cluster,[12–14] and our data provide electronic structure information in support of an atypical nature of A7 by showing that it adopts at least one higher-spin state, as evidenced by the exceptionally broad g ~5.4 feature that exhibited an altered spectral profile in the K165E variant (Fig. 4a, c and Table 1).

It has been reported that the binding and lability of lysine to heme iron in cytochrome *c* variants has a synergistic relationship with protein motions.[48,68,69] While a direct comparison to NfnABC is oversimplistic, the results nevertheless emphasize that lysine-ligation can exert extensive control over protein function (which need not be evident from static structures). In the context of NfnABC, on/off ligation of K165 could control the reduction potentials of A7, thereby dynamically influencing the ΔG° term during A7-A6 and/or A7-FAD ET steps. Indeed, we are not the first to consider redox chemistry control *via* dynamics of A7's lysine ligand.[12] Extreme conformational flexibility, underscored by the breath of A7's g ~5.4 resonance, could also have profound impacts on ΔG° and λ.

4. Conclusions

Our EPR study of *Tsi* NfnABC advances the understanding of the ET relay within this complex EB enzyme. We specifically identified spectral signatures of the A7 cluster within the NfnL-like domain and all three components of the BF-FBC (B1, FMN, and C1). These signatures will be essential for future studies addressing the similarities and differences of EB mechanisms in *Tsi* NfnABC and the broader BfuABC family. By placing our results within the context of ET theory, we identified cofactor properties that we believe need to be considered in such future studies to best understand the operating principles of *Tsi* NfnABC, such as the role of lysine-ligation to A7, and of other BfuABC enzymes, such as functional implications of higher-spin states and of the slow spin–lattice relaxation of the pivotal C1 [2Fe-2S] cluster. Furthermore, future studies should utilize enzyme variants to provide robust Fe–S assignments to the higher-spin states not belonging to A7. Redox titrations will also be important for determining the reduction potentials of cofactors and their influence on discrete ET steps. More broadly, the insight garnered herein regarding how *Tsi* NfnABC and other BfuABC enzymes control ET is applicable to numerous other Fe–S cluster containing enzymes. A collective understanding about the range of ET control in various energy transforming mechanisms is essential for strengthening the design principles of artificial and bioengineered ET processes.

Author contributions

CEL, MWWA, and GEV acquired funding. GEV, GJS, and MWWA designed the study. SW performed wild type enzyme protein expression, purification, and corresponding EPR sample preparations and expressed K165E enzyme. GJS purified K165E enzyme and prepared the corresponding EPR samples. GEV collected, analyzed, and interpreted the data with feedback from all authors. GEV drafted and CEL, MWWA, and GJS edited the manuscript. GEV prepared and CEL edited the final version of the manuscript. All authors have approved the final version of the manuscript.

Conflicts of interest

There are no conflicts to declare.

Data availability

The data supporting this article have been included as part of the supplementary information (SI). Supplementary information: experimental details, Fig. S1–S38, and Tables S1–S15. See DOI: https://doi.org/10.1039/d5dt02921j.

References from the Materials and Methods in the SI that are not cited in the main text are cited here.[70–77]

Acknowledgements

This work was authored in part by NLR for the U.S. Department of Energy (DOE) under Contract No. DE-AC36-08GO28308. GEV was supported in part by a Laboratory Directed Research and Development (LDRD) Director's Fellowship at NLR. Funding for CEL and GEV was provided by the U.S. Department of Energy, Office of Science Early Career Award Program and the U.S. DOE Office of Basic Energy Sciences, Division of Chemical Sciences, Geosciences, and Biosciences, Physical Biosciences Program. This work was also funded in part by a grant (DE-FG02-95ER20175 to MWWA) from the Division of Chemical Sciences, Geosciences and Biosciences, Office of Basic Energy Sciences of the U.S. Department of Energy (SW, GJS, and MWWA). The views expressed in this article do not necessarily represent the views of the DOE or the U.S. government. The U.S. Government retains and the publisher, by accepting the article for publication, acknowledges that the U.S. Government retains a non-exclusive, paid-up, irrevocable, worldwide licenses to publish or reproduce the published form of this work, or allows others to do so, for U.S. Government purposes.

We thank Farris L. Poole (University of Georgia) for assistance with sample preparation and for helpful discussions, Dr Effie C. Kisgeropoulos, Dr Seth A. Wiley, Dr Peter J. Dahl, Dr Syed M.S. Imran, and Michael E. Dawson (NLR) for helpful discussions.

References

1 W. Buckel and R. K. Thauer, Energy conservation via electron bifurcating ferredoxin reduction and proton/Na^+ translocating ferredoxin oxidation, *Biochim. Biophys. Acta, Bioenerg.*, 2013, **1827**(2), 94–113, DOI: 10.1016/j.bbabio.2012.07.002.

2 J. L. Yuly, P. Zhang, X. Ru, K. Terai, N. Singh and D. N. Beratan, Efficient and reversible electron bifurcation with either normal or inverted potentials at the bifurcating cofactor, *Chem*, 2021, **7**(7), 1870–1886, DOI: 10.1016/j.chempr.2021.03.016.

3 S. A. Wiley, I. J. Spackman and C. E. Lubner, Differential ligation alters electronic state and coupling signals of iron-sulfur clusters in flavin-based electron bifurcation, *J. Inorg. Biochem.*, 2026, **274**, 113051, DOI: 10.1016/j.jinorgbio.2025.113051.

4 A. Wójcik-Augustyn, Ł. Bujnowicz, A. Osyczka and M. Sarewicz, Electron bifurcation arises from emergent features of multicofactor enzymes, *ACS Omega*, 2026, DOI: 10.1021/acsomega.5c13233.

5 S. A. Wiley and C. E. Lubner, Photoinduced electron transfer informs on pathway coupling in flavin-based electron bifurcation, *ACS Bio Med Chem Au*, 2026, **6**(1), 78–89, DOI: 10.1021/acsbiomedchemau.5c00232.

6 S. Wang, H. Huang, J. Moll and R. K. Thauer, $NADP^+$ reduction with reduced ferredoxin and $NADP^+$ reduction with NADH are coupled via an electron-bifurcating enzyme complex in *Clostridium kluyveri*, *J. Bacteriol.*, 2010, **192**(19), 5115–5123, DOI: 10.1128/JB.00612-10.

7 F. Kremp, J. Roth and V. Müller, The *Sporomusa* type Nfn is a novel type of electron-bifurcating transhydrogenase that links the redox pools in acetogenic bacteria, *Sci. Rep.*, 2020, **10**, 14872, DOI: 10.1038/s41598-020-71038-2.

8 G. J. Schut, D. K. Haja, X. Feng, F. L. Poole, H. Li and M. W. W. Adams, An abundant and diverse new family of electron bifurcating enzymes with a non-canonical catalytic mechanism, *Front. Microbiol.*, 2022, **13**, 946711, DOI: 10.3389/fmicb.2022.946711.

9 J. K. Demmer, H. Huang, S. Wang, U. Demmer, R. K. Thauer and U. Ermler, Insights into flavin-based electron bifurcation via the NADH-dependent reduced ferredoxin:NADP oxidoreductase structure, *J. Biol. Chem.*, 2015, **290**(36), 21985–21995, DOI: 10.1074/jbc.M115.656520.

10 C. E. Lubner, D. P. Jennings, D. W. Mulder, G. J. Schut, O. A. Zadvornyy, J. P. Hoben, M. Tokmina-Lukaszewska, L. Berry, D. M. Nguyen, G. L. Lipscomb, B. Bothner, A. K. Jones, A.-F. Miller, P. W. King, M. W. W. Adams and J. W. Peters, Mechanistic insights into energy conservation by flavin-based electron bifurcation, *Nat. Chem. Biol.*, 2017, **13**, 655–659, DOI: 10.1038/nchembio.2348.

11 C. E. Wise, A. E. Ledinina, D. W. Mulder, K. J. Chou, J. W. Peters, P. W. King and C. E. Lubner, An uncharacteristically low-potential flavin governs the energy landscape of electron bifurcation, *Proc. Natl. Acad. Sci. U. S. A.*, 2022, **119**(12), e2117882119, DOI: 10.1073/pnas.2117882119.

12 A. Kumar, F. Kremp, J. Roth, S. A. Freibert, V. Müller and J. M. Schuller, Molecular architecture and electron transfer pathway of the Stn family transhydrogenase, *Nat. Commun.*, 2023, **14**, 5484, DOI: 10.1038/s41467-023-41212-x.

13 H. Li, G. J. Schut, X. Feng, M. W. W. Adams and H. Li, Cryo-EM reveals a composite flavobicluster electron bifurcation site in the Bfu family member NfnABC, *Commun. Biol.*, 2025, **8**, 239, DOI: 10.1038/s42003-025-07706-8.

14 X. Xiao, G. J. Schut, X. Feng, D. M. N. Nguyen, H. Huang, S. Wang, H. Li and M. W. W. Adams, Cryo-EM structures define the electron bifurcating flavobicluster and ferredoxin binding site in an archaeal Nfn-Bfu transhydrogenase, *J. Biol. Chem.*, 2025, **301**(4), 108410, DOI: 10.1016/j.jbc.2025.108410.

15 X. Feng, G. J. Schut, S. Putumbaka, H. Li and M. W. Adams, An electron-bifurcating "plug" to a protein nanowire in tungsten-dependent aldehyde detoxification, *Proc. Natl. Acad. Sci. U. S. A.*, 2025, **122**(30), e2501900122, DOI: 10.1073/pnas.2501900122.

16 X. Feng, G. J. Schut, D. K. Haja, M. W. W. Adams and H. Li, Structure and electron transfer pathways of an electron-bifurcating NiFe-hydrogenase, *Sci. Adv.*, 2022, **8**(8), eabm7546, DOI: 10.1126/sciadv.abm7546.

17 C. Furlan, N. Chongdar, P. Gupta, W. Lubitz, H. Ogata, J. N. Blaza and J. A. Birrell, Structural insight on the mechanism of an electron-bifurcating [FeFe] hydrogenase, *eLife*, 2022, **11**, e79361, DOI: 10.7554/eLife.79361.

18 A. Katsyv, A. Kumar, P. Saura, M. C. Pöverlein, S. A. Freibert, S. T. Stripp, S. Jain, A. P. Gamiz-Hernandez, V. R. I. Kaila, V. Müller and J. M. Schuller, Molecular basis of the electron bifurcation mechanism in the [FeFe]-hydrogenase complex HydABC, *J. Am. Chem. Soc.*, 2023, **145**(10), 5696–5709, DOI: 10.1021/jacs.2c11683.

19 E. Babini, I. Bertini, M. Borsari, F. Capozzi, C. Luchinat, X. Zhang, G. L. C. Moura, I. V. Kurnikov, D. N. Beratan, A. Ponce, A. J. Di Bilio, J. R. Winkler and H. B. Gray, Bond-mediated electron tunneling in ruthenium-modified high-potential iron–sulfur protein, *J. Am. Chem. Soc.*, 2000, **122**(18), 4532–4533, DOI: 10.1021/ja994472t.

20 P. Bertrand, C. More and P. Camensuli, Evidence for a magic magnetic configuration between FMN and the $[2Fe\text{-}2S]^+$ center of phthalate dioxygenase reductase of *Pseudomonas cepacia*, *J. Am. Chem. Soc.*, 1995, **117**(6), 1807–1809, DOI: 10.1021/ja00111a020.

21 M. Boll, G. Fuchs and D. J. Lowe, Single turnover EPR studies of benzoyl-CoA reductase, *Biochemistry*, 2001, **40**(25), 7612–7620, DOI: 10.1021/bi002771l.

22 C. E. Lubner, J. H. Artz, D. W. Mulder, A. Oza, R. J. Ward, S. G. Williams, A. K. Jones, J. W. Peters, I. I. Smalyukh, V. S. Bharadwaj and P. W. King, A site-differentiated [4Fe–4S] cluster controls electron transfer reactivity of *Clostridium acetobutylicum* [FeFe]-hydrogenase I, *Chem. Sci.*, 2022, **13**, 4581–4588, DOI: 10.1039/D1SC07120C.

23 P. A. Lindahl, N. J. Gorelick, E. Münck and W. H. Orme-Johnson, EPR and Mössbauer studies of nucleotide-bound nitrogenase iron protein from *Azotobacter vinelandii*, *J. Biol.*

Chem., 1987, **262**(31), 14945–14953, DOI: 10.1016/S0021-9258(18)48120-3.

24 M. Sarewicz, M. Dutka, R. Pietras, A. Borek and A. Osyczka, Effect of H bond removal and changes in the position of the iron–sulphur head domain on the spin–lattice relaxation properties of the $[2Fe–2S]^{2+}$ Rieske cluster in cytochrome bc_1, *Phys. Chem. Chem. Phys.*, 2015, **17**, 25297–25308, DOI: 10.1039/C5CP02815A.

25 K. Zuchan, F. Baymann, C. Baffert, M. Brugna and W. Nitschke, The dyad of the Y-junction- and a flavin module unites diverse redox enzymes, *Biochim. Biophys. Acta, Bioenerg.*, 2021, **1862**(6), 148401, DOI: 10.1016/j.bbabio.2021.148401.

26 S. Huang, S. M. S. Imran, A. A. Lanahan, S. K. Hammer, C. E. Lubner, L. R. Lynd and D. G. Olson, A distinct class of ferredoxin:$NADP^+$ oxidoreductase enzymes driving thermophilic ethanol production, *J. Biol. Chem.*, 2025, **301**(7), 110263, DOI: 10.1016/j.jbc.2025.110263.

27 S. G. Mayhew, The redox potential of dithionite and SO_2^- from equilibrium reactions with flavodoxins, methyl viologen and hydrogen plus hydrogenase, *Eur. J. Biochem.*, 1978, **85**(2), 535–547, DOI: 10.1111/j.1432-1033.1978.tb12269.x.

28 R. Cammack, Iron—sulfur clusters in enzymes: themes and variations, *Adv. Inorg. Chem.*, 1992, **38**, 281–322, DOI: 10.1016/S0898-8838(08)60066-5.

29 R. Mathews, S. Charlton, R. H. Sands and G. Palmer, On the nature of the spin coupling between the iron-sulfur clusters in the eight-iron ferredoxins, *J. Biol. Chem.*, 1974, **249**(13), 4326–4328, DOI: 10.1016/S0021-9258(19)42521-0.

30 Z. Dermoun, G. De Luca, M. Asso, P. Bertrand, F. Guerlesquin and B. Guigliarelli, The NADP-reducing hydrogenase from *Desulfovibrio fructosovorans*: functional interaction between the C-terminal region of HndA and the N-terminal region of HndD subunits, *Biochim. Biophys. Acta, Bioenerg.*, 2002, **1556**(2–3), 217–225, DOI: 10.1016/S0005-2728(02)00364-X.

31 J. R. Harmer, S. Hakopian, D. Niks, R. Hille and P. V. Bernhardt, Redox characterization of the complex molybdenum enzyme formate dehydrogenase from *Cupriavidus necator*, *J. Am. Chem. Soc.*, 2023, **145**(47), 25850–25863, DOI: 10.1021/jacs.3c10199.

32 K. Zuchan, N. Breuer, C. Laurich, W. Nitschke, F. Baymann and J. A. Birrell, Thermodynamic landscape of the redox-centres in the electron-confurcating [FeFe]-hydrogenase (*Tm*HydABC) of *Thermotoga maritima*, *Biochim. Biophys. Acta, Bioenerg.*, 2026, **1867**(2), 149577, DOI: 10.1016/j.bbabio.2025.149577.

33 D. M. Duggan and D. N. Hendrickson, Magnetic exchange interactions in transition metal dimers. III. Nickel(II) di-μ-cyanato, di-μ-thiocyanato, and di-μ-selenocyanato complexes and related outer-sphere copper(II) complexes, *Inorg. Chem.*, 1974, **13**(12), 2929–2940, DOI: 10.1021/ic50142a031.

34 W. R. Hagen, *Biomolecular EPR Spectroscopy*, CRC Press, 2009.

35 A. Juszczak, S. Aono and M. W. W. Adams, The extremely thermophilic eubacterium, *Thermotoga maritima*, contains a novel iron-hydrogenase whose cellular activity is dependent upon tungsten, *J. Biol. Chem.*, 1991, **266**(21), 13834–13841, DOI: 10.1016/S0021-9258(18)92777-8.

36 I. C. Zambrano, A. T. Kowal, L. E. Mortenson, M. W. W. Adams and M. K. Johnson, Magnetic circular dichroism and electron paramagnetic resonance studies of hydrogenases I and II from *Clostridium pasteurianum*, *J. Biol. Chem.*, 1989, **264**(35), 20974–20983, DOI: 10.1016/S0021-9258(19)30032-8.

37 J. W. Peters, W. N. Lanzilotta, B. J. Lemon and L. C. Seefeldt, X-ray crystal structure of the Fe-only hydrogenase (CpI) from *Clostridium pasteurianum* to 1.8 angstrom resolution, *Science*, 1998, **282**(5395), 1853–1858, DOI: 10.1126/science.282.5395.1853.

38 M.-F. Jeng, S. W. Englander, K. Pardue, J. S. Rogalskyj and G. McLendon, Structural dynamics in an electron–transfer complex, *Nat. Struct. Biol.*, 1994, **1**, 234–238, DOI: 10.1038/nsb0494-234.

39 S. Subramanian, E. C. Duin, S. E. J. Fawcett, F. A. Armstrong, J. Meyer and M. K. Johnson, Spectroscopic and redox studies of valence-delocalized $[Fe_2S_2]^+$ centers in thioredoxin-like ferredoxins, *J. Am. Chem. Soc.*, 2015, **137**(13), 4567–4580, DOI: 10.1021/jacs.5b01869.

40 B. A. Skeel and D. L. M. Suess, Iron-sulfur clusters: the road to room temperature, *J. Biol. Inorg. Chem.*, 2025, **30**, 151–159, DOI: 10.1007/s00775-025-02094-0.

41 W. R. Hagen, EPR spectroscopy of iron—sulfur proteins, *Adv. Inorg. Chem.*, 1992, **38**, 165–222, DOI: 10.1016/S0898-8838(08)60064-1.

42 W. R. Hagen, H. Wassink, R. R. Eady, B. E. Smith and H. Haaker, Quantitative EPR of an S = 7/2 system in thionine-oxidized MoFe proteins of nitrogenase: a redefinition of the P-cluster concept., *Eur. J. Biochem.*, 1987, **169**(3), 457–465, DOI: 10.1111/j.1432-1033.1987.tb13633.x.

43 M. Boll, S. S. P. Albracht and G. Fuchs, Benzoyl-CoA reductase (dearomatizing), a key enzyme of anaerobic aromatic metabolism: a study of adenosinetriphosphatase activity, ATP stoichiometry of the reaction and EPR properties of the enzyme, *Eur. J. Biochem.*, 1997, **244**(3), 840–851, DOI: 10.1111/j.1432-1033.1997.00840.x.

44 D. Prakash, J. Xiong, S. S. Chauhan, K. A. Walters, H. Kruse, N. Yennawar, J. H. Golbeck, Y. Guo and J. G. Ferry, Catalytic activity of the archetype from Group 4 of the FTR-like ferredoxin:thioredoxin reductase family is regulated by unique S = 7/2 and S = 1/2 [4Fe–4S] clusters, *Biochemistry*, 2024, **63**(12), 1588–1598, DOI: 10.1021/acs.biochem.3c00651.

45 M. Ye, A. C. Brown and D. L. M. Suess, Reversible alkyl-group migration between iron and sulfur in $[Fe_4S_4]$ clusters, *J. Am. Chem. Soc.*, 2022, **144**(29), 13184–13195, DOI: 10.1021/jacs.2c03195.

46 J. Gaillard, J. M. Moulis, P. Auric and J. Meyer, High-multiplicity spin states of $2[4Fe\text{-}4Se]^+$ clostridial ferredoxins, *Biochemistry*, 1986, **25**(2), 464–468, DOI: 10.1021/bi00350a028.

47 W. R. Hagen, Wide zero field interaction distributions in the high-spin EPR of metalloproteins, *Mol. Phys.*, 2007, **105**(15–16), 2031–2039, DOI: 10.1080/00268970701558570.

48 F. Zhong, S. L. Alden, R. P. Hughes and E. V. Pletneva, Comparing properties of common bioinorganic ligands with switchable variants of cytochrome *c*, *Inorg. Chem.*, 2022, **61**(3), 1207–1227, DOI: 10.1021/acs.inorgchem.1c02322.

49 D. Nohr, S. Weber and E. Schleicher, EPR spectroscopy on flavin radicals in flavoproteins, *Methods Enzymol.*, 2019, **620**, 251–275, DOI: 10.1016/bs.mie.2019.03.013.

50 K. Zuchan, W. Nitschke, F. Baymann, N. Breuer and J. Birrell, NAD(H)-induced flavosemiquinone stabilization in the electron-confurcating [FeFe]-hydrogenase (HydABC) of *Thermotoga maritima*, *Biochim. Biophys. Acta, Bioenerg.*, 2022, **1863**, 148758, DOI: 10.1016/j.bbabio.2022.148758.

51 T. Young, D. Niks, S. Hakopian, T. K. Tam, X. Yu, R. Hille and G. M. Blaha, Crystallographic and kinetic analyses of the FdsBG subcomplex of the cytosolic formate dehydrogenase FdsABG from *Cupriavidus necator*, *J. Biol. Chem.*, 2020, **295**(19), 6570–6585, DOI: 10.1074/jbc.RA120.013264.

52 A. Fournel, S. Gambarelli, B. Guigliarelli, C. More, M. Asso, G. Chouteau, R. Hille and P. Bertrand, Magnetic interactions between a $[4Fe–4S]^{1+}$ cluster and a flavin mononucleotide radical in the enzyme trimethylamine dehydrogenase: a high-field electron paramagnetic resonance study, *J. Chem. Phys.*, 1998, **109**(24), 10905–10913, DOI: 10.1063/1.477786.

53 J. Blumberger, Recent advances in the theory and molecular simulation of biological electron transfer reactions, *Chem. Rev.*, 2015, **115**(20), 11191–11238, DOI: 10.1021/acs.chemrev.5b00298.

54 R. A. Marcus and N. Sutin, Electron transfers in chemistry and biology, *Biochim. Biophys. Acta, Rev. Bioenerg.*, 1985, **811**(3), 265–322, DOI: 10.1016/0304-4173(85)90014-X.

55 P. Bertrand, Application of electron transfer theories to biological systems, in *Structure and Bonding, Long-Range Electron Transfer in Biology*, Springer, Berlin Heidelberg, 1991, vol. 75, pp. 1–47.

56 J.-P. Gayda, P. Bertrand, A. Deville, C. More, G. Roger, J. F. Gibson and R. Cammack, Temperature dependence of the electronic spin-lattice relaxation time in a 2-iron-2-sulfur protein, *Biochim. Biophys. Acta, Protein Struct.*, 1979, **581**(1), 15–26, DOI: 10.1016/0005-2795(79)90216-2.

57 M. G. I. Galinato, S. E. Bowman, J. G. Kleingardner, S. Martin, J. Zhao, W. Sturhahn, E. E. Alp, K. L. Bren and N. Lehnert, Effects of protein structure on iron–polypeptide vibrational dynamic coupling in cytochrome *c*, *Biochemistry*, 2015, **54**(4), 1064–1076, DOI: 10.1021/bi501430z.

58 D. V. Matyushov, Protein electron transfer: is biology (thermo) dynamic?, *J. Phys.:Condens. Matter*, 2015, **27**(47), 473001, DOI: 10.1088/0953-8984/27/47/473001.

59 Y. Huang, C. T. Rettner, D. J. Auerbach and A. M. Wodtke, Vibrational promotion of electron transfer, *Science*, 2000, **290**(5489), 111–114, DOI: 10.1126/science.290.5489.111.

60 J. Gaillard, J. M. Moulis and J. Meyer, Hydrogen-1 nuclear magnetic resonance of selenium-substituted clostridial ferredoxins, *Inorg. Chem.*, 1987, **26**(2), 320–324, DOI: 10.1021/ic00249a021.

61 J. Meyer, J. Gaillard and J. M. Moulis, Hydrogen-1 nuclear magnetic resonance of the nitrogenase iron protein (Cp2) from *Clostridium pasteurianum*, *Biochemistry*, 1988, **27**(16), 6150–6156, DOI: 10.1021/bi00416a048.

62 S. Sharma, K. Sivalingam, F. Neese and G. K.-L. Chan, Low-energy spectrum of iron–sulfur clusters directly from many-particle quantum mechanics, *Nat. Chem.*, 2014, **6**, 927–933, DOI: 10.1038/nchem.2041.

63 E. L. Bominaar, C. Achim and S. A. Borshch, Theory for electron transfer from a mixed-valence dimer with paramagnetic sites to a mononuclear acceptor, *J. Chem. Phys.*, 1999, **110**(23), 11411–11422, DOI: 10.1063/1.479082.

64 A. Kubas, How the donor/acceptor spin states affect the electronic couplings in molecular charge-transfer processes?, *J. Chem. Theory Comput.*, 2021, **17**(5), 2917–2927, DOI: 10.1021/acs.jctc.1c00126.

65 M. J. Carney, G. C. Papaefthymiou, R. B. Frankel and R. H. Holm, Alternative spin states in synthetic analogs of biological iron-sulfur $[4Fe\text{-}4S]^{+}$ clusters: further cases of variable ground states and the structure of $(Et_4N)_3[Fe_4S_4(S\text{-}o\text{-}C_6H_4S\text{-}tert\text{-}Bu)_4]$, containing a reduced cluster with a compressed tetragonal distortion, *Inorg. Chem.*, 1989, **28**(8), 1497–1503, DOI: 10.1021/ic00307a015.

66 Y. A. Onate, M. G. Finnegan, B. J. Hales and M. K. Johnson, Variable temperature magnetic circular dichroism studies of reduced nitrogenase iron proteins and $[4Fe\text{-}4S]^{+}$ synthetic analog clusters, *Biochim. Biophys. Acta, Protein Struct. Mol. Enzymol.*, 1993, **1164**(2), 113–123, DOI: 10.1016/0167-4838(93)90237-L.

67 O. Einsle and D. C. Rees, Structural enzymology of nitrogenase enzymes, *Chem. Rev.*, 2020, **120**(12), 4969–5004, DOI: 10.1021/acs.chemrev.0c00067.

68 J. F. Amacher, F. Zhong, G. P. Lisi, M. Q. Zhu, S. L. Alden, K. R. Hoke, D. R. Madden and E. V. Pletneva, A compact structure of cytochrome *c* trapped in a lysine-ligated state: loop refolding and functional implications of a conformational switch, *J. Am. Chem. Soc.*, 2015, **137**(26), 8435–8449, DOI: 10.1021/jacs.5b01493.

69 J. Gu, D.-W. Shin and E. V. Pletneva, Remote perturbations in tertiary contacts trigger ligation of lysine to the heme iron in cytochrome *c*, *Biochemistry*, 2017, **56**(23), 2950–2966, DOI: 10.1021/acs.biochem.6b01187.

70 S. Aono, F. O. Bryant and M. W. Adams, A novel and remarkably thermostable ferredoxin from the hyperthermophilic archaebacterium *Pyrococcus furiosus*, *J. Bacteriol.*, 1989, **171**(6), 3433–3439, DOI: 10.1128/jb.171.6.3433-3439.1989.

71 S. Stoll and A. Schweiger, EasySpin, a comprehensive software package for spectral simulation and analysis in EPR, *J. Magn. Reson.*, 2006, **178**(1), 42–55, DOI: 10.1016/j.jmr.2005.08.013.

72 G. R. Eaton, S. S. Eaton, D. P. Barr and R. T. Weber, *Quantitative EPR*, Springer-Verlag/Wein, 2010.

73 G. W. Brudvig, Electron paramagnetic resonance spectroscopy, *Methods Enzymol.*, 1995, **246**, 536–554, DOI: 10.1016/0076-6879(95)46024-1.

74 T. U. Consortium, UniProt: the universal protein knowledgebase in 2023, *Nucleic Acids Res.*, 2022, **51**(D1), D523–D531, DOI: 10.1093/nar/gkac1052.

75 F. Sievers, A. Wilm, D. Dineen, T. J. Gibson, K. Karplus, W. Li, R. Lopez, H. McWilliam, M. Remmert, J. Söding, J. D. Thompson and D. G. Higgins, Fast, scalable generation of high-quality protein multiple sequence alignments using Clustal Omega, *Mol. Syst. Biol.*, 2011, **7**, MSB201175, DOI: 10.1038/msb.2011.75.

76 A. M. Waterhouse, J. B. Procter, D. M. A. Martin, M. Clamp and G. J. Barton, Jalview Version 2—a multiple sequence alignment editor and analysis workbench, *Bioinformatics*, 2009, **25**(9), 1189–1191, DOI: 10.1093/bioinformatics/btp033.

77 W. L. DeLano, Pymol: An open-source molecular graphics tool, *CCP4 Newsl. Protein Crystallogr.*, 2002, **40**(1), 82–92.